CONDENSED
MATTER

Wave-Packet Dynamics Study of the Transport Characteristics of Perforated Bilayer Graphene Nanoribbons

V. A. Demin[a], **D. G. Kvashnin**[a], **P. Vancsó**[b], **G. I. Márk**[b], and **L. A. Chernozatonskii**[a, c, *]

[a] *Emanuel Institute of Biochemical Physics, Russian Academy of Sciences, Moscow, 119334 Russia*
[b] *Institute of Technical Physics and Materials Science, Centre for Energy Research,*
H-1525 Budapest, Hungary
[c] *Scientific School on Chemistry and Technology of Polymer Materials,*
Plekhanov Russian University of Economics, Moscow, 117997 Russia
*e-mail: chernol-43@mail.ru

The electrical conduction characteristics of perforated bilayer graphene nanoribbons are studied by the wave-packet dynamics method. The transport characteristics for typical examples of such nanostructures, which depend on the specific features of the contacts between the electrodes and the nanostructure under study, are estimated within a theoretical model. The effect of nanopores on the propagation of a wave packet across bilayer nanoribbons having two different configurations is revealed. These studies may become the first necessary prerequisite for the possible applications of such objects as components of electronic and optoelectronic circuits.

INTRODUCTION

Graphene nanoribbons (GNRs) are one-dimensional graphene strips with the optical, electronic, and magnetic properties determined by their width and edge structure. Graphene nanoribbons with zigzag edges are metals [1], and those with armchair edges are semiconductors with the band gap depending on their width [2]. It is also possible to control the electronic characteristics of graphene nanoribbons by their distortion [3] or by the adsorption of atoms on their surface [4]. The dependence of the band gap in GNRs on their structure makes them ideal objects for application as connectors. Owing to this feature, GNR-based electronic devices can become efficient substitutes for the silicon analogs in new generation nanodevices. Currently, the possibilities of using GNRs as various electronic components are being actively investigated [5]. Modern technologies already allow synthesis of GNRs with a width of several tenths of nanometer by various techniques, such as electron lithography, cutting nanotubes, and self-assembly of molecules [6].

In addition to monolayer structures, bilayer graphene nanosystems, in which the dispersion relation of charge carriers has a quadratic form in contrast to that of single-layer graphene, are of particular interest [7]. Note that the electronic properties of bilayer graphene can be easily controlled, for example, by

applying an electric field [8, 9] or by molecular adsorption [10, 11].

A promising line of research suggesting the possibility of controlling the electronic properties of graphene-based nanostructures is the formation of nanopores [12]. In contrast to pores in monolayer graphene, nanopores in bilayer graphene are closed, which leads to certain specific features of their electronic characteristics, as well as to their chemical stability in the presence of only topological defects at the nanopore boundary [13–15]. Moreover, it was predicted earlier that the joining of edges in a nanopore of bilayer graphene is a spontaneous process [14]. The formation of such type of arrays was recently confirmed in experiments [16, 17]. In addition, the possibility of a semimetal–semiconductor transition is demonstrated in [18] using three-layer graphene systems with pores as specific examples. All this makes porous multilayer graphene an extremely interesting object for the studies on specific features of their characteristics, having in mind their promising applications in future nanoelectronics.

Similar to bilayer graphene with periodic nanopore arrays, bilayer GNRs with nanopores are also of particular interest as a new class of quasi-one-dimensional carbon materials. As in the case of single-layer GNRs, charge carriers in bilayer GNRs are also limited in their motion along two spatial directions. The electronic characteristics of such arrays can also be

controlled by changing their width [19, 20]. In addition, it was shown that the electronic and transport characteristics of bilayer GNRs strongly depend on the voltage applied across the layers [19−21]; this was also demonstrated in experiments [22]. Thus, the presence of nanopores in bilayer GNRs can significantly affect their physical and chemical properties, which requires a thorough fundamental study.

In this work, we study the electrical conduction characteristics of bilayer graphene nanoribbons with nanopores by simulating the propagation of an electron wave packet along them.

RESEARCH TECHNIQUES

The wave-packet (WP) dynamics method is a computer simulation of the propagation of a WP through a localized potential relief [23]. The time dependence of WP propagation is calculated by solving the time-dependent Schrödinger equation. The result of calculating the WP dynamics gives a detailed information on the WP propagation process with the course of time.

The model system consists of an electrode generating the WP, the localized potential relief forming the array under study, and an absorbing potential. The metal electrode is described as an electron gas having the Fermi energy $E_F = 5$ eV and work function $W = 4.81$ eV. The initial kinetic energy of the WP is $E_k = 5$ eV. The pseudopotential related to each sp^2 carbon atom has the form $V(r) = \sum A_i \exp(-a_i r^2)$ with the coefficients $A_1 = 10.607$ eV, $A_2 = 29.711$ eV, and $A_3 = 98.911$ eV and the parameters $a_1 = 0.12126$, $a_2 = 1.9148$, and $a_3 = 0.60078$ in units of r_{Bohr}^{-2} [24]. This pseudopotential was developed for graphene and graphite, but it can also be successfully applied to arrays with sp^2 hybridization containing defects [25−28]. After leaving the electrode, the WP propagates along the constructed localized potential relief toward the absorbing potential without any reflection. The solution of the time-dependent Schrödinger equation is represented as a set of wavefunctions $\psi(r, t)$. Next, we perform the Fourier transform $\psi(r, t) \rightarrow \psi(r, E)$ to separate the WP energies. The found function $\psi(r, E)$ is independent of time, so we can visualize the propagation pattern for the WP component corresponding to a fixed energy. Earlier, this technique was used to study characteristic features of electron transport in carbon nanotubes [29], across graphene grain boundaries [30], and in bigraphene nanomeshes [14].

The atomic structure of bilayer GNRs is calculated by the molecular dynamics method implemented in the LAMMPS software package [31] using the adaptive intermolecular reactive empirical band order (AIREBO) potential [32]. Optimization of the geometry is carried out until the forces acting on each atom become smaller than 10^{-4} eV/Å.
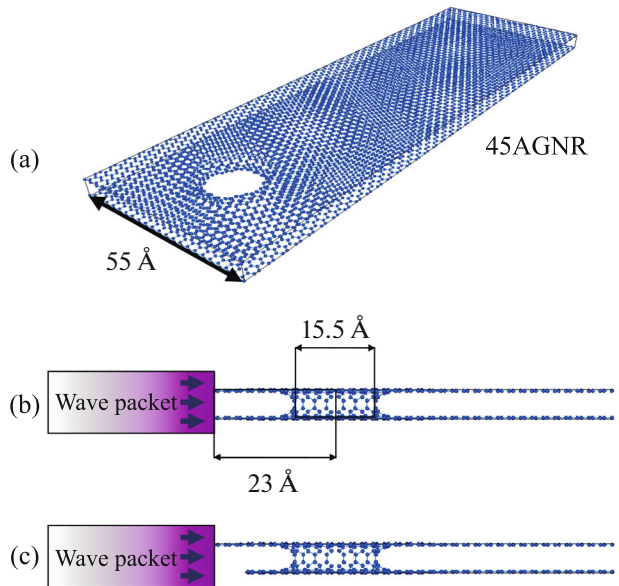

Fig. 1. (Color online) (a) General view of the bilayer 45AGNR nanoribbon with a hole 15.5 Å in diameter; (b, c) types of connections between the nanoribbon and the electrode through which the WP enters the nanoribbon.

RESULTS AND DISCUSSION

As a model system, we choose a 55-Å-wide bilayer armchair graphene nanoribbon (45AGNR) with a hexagonal nanopore 15.5 Å in diameter, whose edges are covalently connected to each other (Fig. 1). The presence of the nanopore affects the interlayer distance, which becomes equal to 5.2 Å after optimization. To study the effect of the nanopore on the conduction characteristics of the bilayer GNR, we consider two types of electrode−ribbon contact: the electrode is connected (i) directly to both layers of the ribbon (Fig. 1b) and (ii) only to the upper layer the bilayer GNR (Fig. 1c). The electrode is located at the distance $L = 23$ Å from the center of the nanopore. The transport characteristics are measured before the time when WP reaches the nanopore and after the passage of the nanopore. The corresponding cross sections are located at distances of 4.35 Å upstream and downstream of the pore.

First, we consider case (i) where the electrode is connected to both layers of the bilayer GNR. To obtain a pattern characterizing the distribution of electron wavefunctions after the WP propagation, we solve the time-dependent Schrödinger equation and, as a result, find sets of wavefunctions $\psi(r, t)$. These wavefunctions squared at times $t = 0.3$ and 4.2 fs are shown in Figs. 2a and 2b, respectively. At time $t = 0.3$ fs, the WP is located at the electrode (Fig. 2a), then the packet propagates along the ribbon, and after 1.5 fs reaches cross section 1, which is chosen to be in front of the nanopore. After that, the WP interacts with the pore and, as a result, a part of the WP becomes local-
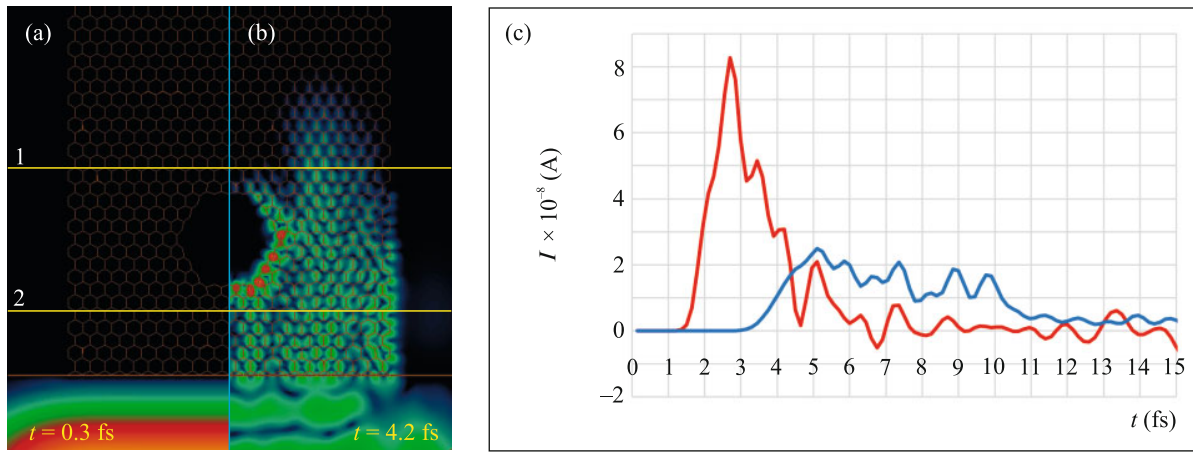
Fig. 2. (Color online) Wave-packet probability densities at times $t =$ (a) 0.3 and (b) 4.2 fs and (c) time dependence of the electric current flowing across crossing planes (red curve) *1* and (blue curve) *2*.
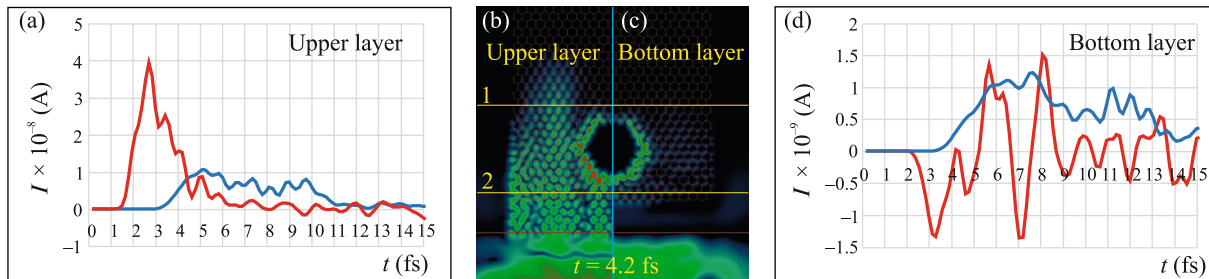

Fig. 3. (Color online) Time dependence of the electric current flowing (a) along the upper layer of the bilayer nanoribbon connected to the electrode and (d) along the lower layer across crossing planes (red curves) *1* and (blue curves) *2*. Wave-packet probability densities at time $t =$ 4.2 fs (b) on the upper layer connected to the electrode and (c) on the free lower layer.

ized at curved regions of the nanopore (bright red areas in Fig. 2b). At time $t =$ 3 fs, the WP reaches cross section 2. For each of these two cross sections, we record the time dependence of the current passing across them (Fig. 2c). Since the GNR is a bilayer system with the AA packing of the layers, and the electrode is connected to both layers, the WP propagates along both layers in the same manner and contributes similarly to the current flowing along these cross sections. The time dependence (Figs. 2c and 2d) demonstrates that the amplitude of electric current exhibits a significant decrease after the WP passage across the nanopore. Such decrease is due to the WP–pore interaction, giving rise to a substantial reverse current.

Next, we consider the second case, where the electrode is connected only to the upper layer of the bilayer GNR (Fig. 1c). In this case, a different picture of the WP propagation is observed (Figs. 3b and 3c). Figure 3 shows the WP probability densities on the (b) upper and (c) lower layers, as well as the time dependence of the electric current recorded at the (a) first and (d) second cross sections. It was found that the WP passes along the upper layer and then becomes split during the passage of the nanopore: a certain por-

tion of it propagates further along the upper layer, whereas the other portion passes through the interlayer bonds within the pore and enters the second layer. According to the time dependence of the electric current, the behavior of the WP in the layer connected to the electrode is similar to that shown in Fig. 2c. The second layer can be considered as a separate system, into which the WP enters through atoms located at the nanopore boundary. The WP propagates in all directions. The blue curve in Fig. 3d demonstrates that some portion of the packet propagates along the nanoribbon from the electrode. At the same time, the other portion of the WP moves toward the electrode; this is illustrated by negative values of the electric current flowing across the first cross section (red curve in Fig. 3d). The electric current flowing across the first cross section oscillates owing to the reflection from the free edge of the ribbon, not attached to the electrode, as well as from the nanopore itself. Oscillations depend on the shape of the free edge of the ribbon, as well as on its distance from the nanopore. Note that the currents flowing along the second layer differ in amplitude by an order of magnitude from those flowing along the layer attached to the electrode (Fig. 3d). Thus, after the WP passage through the nanopore, one
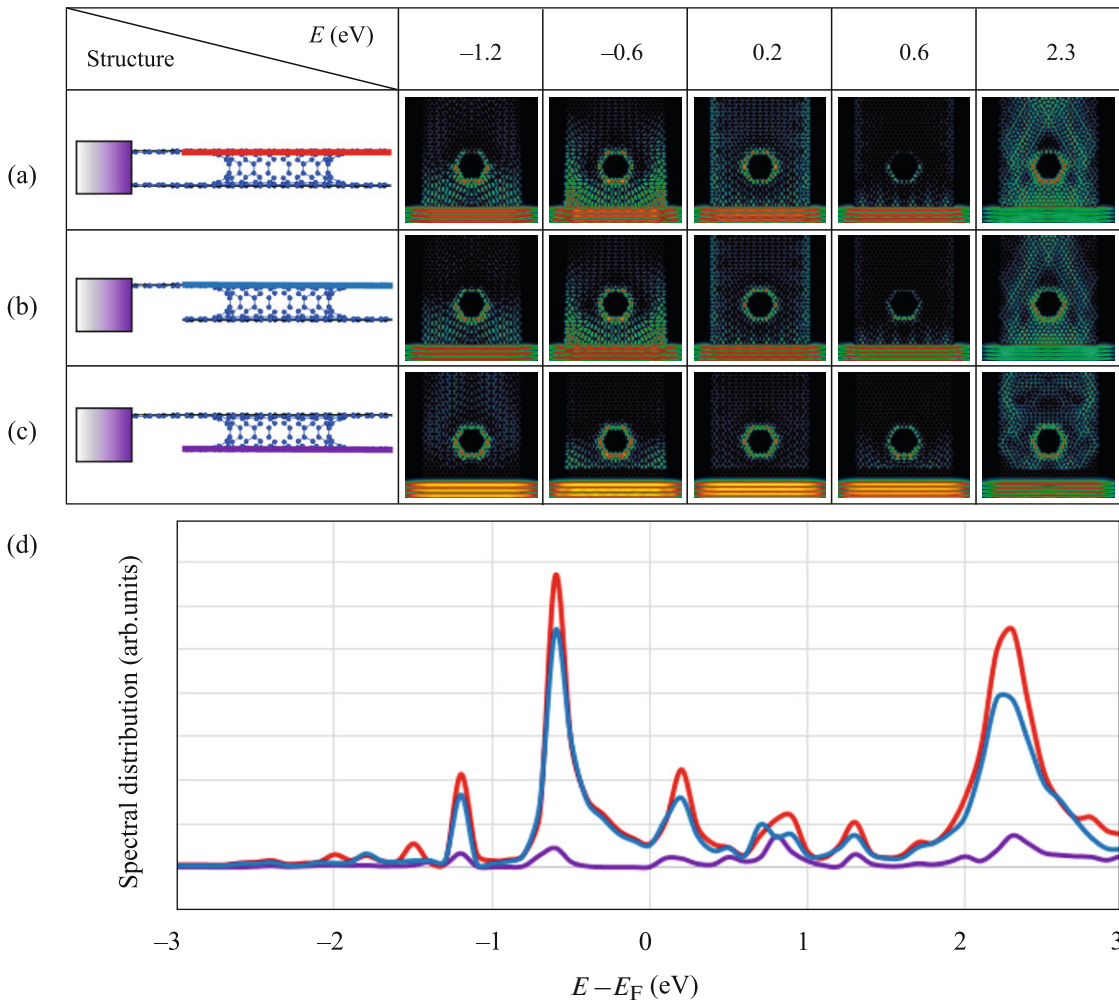
Structure	E (eV) −1.2	−0.6	0.2	0.6	2.3
(a)					
(b)					
(c)					

(d)

Fig. 4. (Color online) (a−c) Wave-packet probability densities corresponding to some peaks of the spectral distribution shown in panel (d). Wave-packet probability densities are shown for one layer: (a) in the case of the electrode connected to both layers and (b, c) in the case of the electrode connected to only one layer for connected and not connected layers, respectively.

portion of it propagates further along the attached ribbon, whereas the other one is localized at the pore boundary and passes to the layer, which is not connected to the electrode. In this case, a significant part of the intensity is lost.

For a more detailed analysis of the WP propagation through the bilayer GNR with the nanopore, we perform the Fourier transform $\psi(r, t) \to \psi(r, E)$ to distinguish WPs with different energies. This makes it possible to obtain a time-independent spectral distribution for WPs. In Fig. 4, we show such spectral distributions for the cases of electrode attachment to both layers and only to the upper layer. Spectral distributions show that the bilayer 45AGNR with the nanopore is metallic. It is important that the existence of the nanopore does not change the type of conductivity, since the same bilayer GNR with a perfect structure also exhibits metallic characteristics. In Fig. 4, we show the probability density distributions for given WP energies, which can be used to determine the energies of localized and delocalized electronic states. The WP

behaves approximately in the same manner in the layers attached to the electrode. However, not all wave packet components corresponding to fixed energies penetrate the layer which is not connected to the electrode. The analysis of the peaks in the spectral distribution shows that the WP at energies $E = -1.2$ and -0.6 eV does not propagate beyond the nanopore and the main part of it becomes localized at distorted bonds located at the nanopore boundaries. At higher energies $E = 0.2$ and 2.3 eV, the WP passes across the edges of the nanopore into the second layer and further on propagates along the ribbon. Thus, it is shown that, by changing the voltage applied across the electrodes, it is possible to control the transmission, delay, or reflection of the WP and hence to control also the electric pulses of different energies being input to the devices (Figs. 1b and 1c). This phenomenon can be used in nanoelectronic pulse devices.

The data obtained suggest that nanopores in bilayer arrays play an important role in the formation of metallic conductivity and of additional steady-state

levels localized directly at the interlayer connection region related to the nanopore. This determines different kinds of electric pulse propagation in perforated bilayer GNRs.

CONCLUSIONS

In this work, we have studied the electrical conduction characteristics of novel quasi-one-dimensional materials based on bilayer graphene nanoribbons with nanopores. Using the wave-packet dynamics method, we have demonstrated the metallic type conductivity in a bilayer graphene nanoribbon with a nanopore. The presence of a nanopore favors the formation of localized electronic states at its boundary. Moreover, it has been shown that an important parameter here is the type of connection between the nanoribbon and the electrode. The connection with only one layer leads to a significant change in the transport characteristics; namely, in such systems, a nanopore serves as a signal divider. The time dependences of the electric current measured after the passage of a wave packet across the nanopore are significantly different for different layers. Both the size and shape of the pore and the geometry of the nanoribbon edge not connected to the electrode affect these dependences. This leads to the possibility of controlled passage of electric pulses through the nanostructures under study and is important for their potential applications in nanoelectronics.

FUNDING

REFERENCES

1. Y.-W. Son, M. L. Cohen, and S. G. Louie, Nature (London, U. K.) **444**, 347 (2006).
2. Y.-W. Son, M. L. Cohen, and S. G. Louie, Phys. Rev. Lett. **97**, 216803 (2006).
3. A. V. Zhukov, R. Bouffanais, N. N. Konobeeva, and M. B. Belonenko, JETP Lett. **97**, 400 (2013).
4. L. A. Chernozatonskii, A. A. Artyukh, and D. G. Kvashnin, JETP Lett. **95**, 266 (2012).
5. J. M. Marmolejo-Tejada and J. Velasco-Medina, Microelectron. J. **48**, 18 (2016).
6. A. Celis, M. N. Nair, A. Taleb-Ibrahimi, E. H. Conrad, C. Berger, W. A. de Heer, and A. Tejeda, J. Phys. D: Appl. Phys. **49**, 143001 (2016).
7. A. H. Castro Neto, F. Guinea, N. M. R. Peres, K. S. Novoselov, and A. K. Geim, Rev. Mod. Phys. **81**, 109 (2009).
8. Y. Zhang, T.-T. Tang, C. Girit, Z. Hao, M. C. Martin, A. Zettl, M. F. Crommie, Y. R. Shen, and F. Wang, Nature (London, U. K.) **459**, 820 (2009).
9. Z. Z. Alisultanov, JETP Lett. **103**, 598 (2016).
10. T. Ohta, A. Bostwick, T. Seyller, K. Horn, and E. Rotenberg, Science (Washington, DC, U. S.) **313**, 951 (2006).
11. W. Zhang, C.-T. Lin, K.-K. Liu, T. Tite, C.-Y. Su, C.-H. Chang, Y.-H. Lee, C.-W. Chu, K.-H. Wei, J.-L. Kuo, and L.-J. Li, ACS Nano **5**, 7517 (2011).
12. W. Oswald and Z. Wu, Phys. Rev. B **85**, 115431 (2012).
13. L. A. Chernozatonskii, V. A. Demin, and A. A. Artyukh, JETP Lett. **99**, 309 (2014).
14. D. G. Kvashnin, P. Vancsó, L. Y. Antipina, G. I. Márk, L. P. Biró, P. B. Sorokin, and L. A. Chernozatonskii, Nano Res. **8**, 1250 (2015).
15. L. A. Chernozatonskii, V. A. Demin, and Ph. Lambin, Phys. Chem. Chem. Phys. **18**, 27432 (2016).
16. K. He, A. W. Robertson, C. Gong, C. S. Allen, Q. Xu, H. Zandbergen, J. C. Grossman, A. I. Kirkland, and J. H. Warner, Nanoscale **7**, 11602 (2015).
17. N. A. Nebogatikova, I. V. Antonova, S. V. Erohin, D. G. Kvashnin, A. Olejniczak, V. A. Volodin, A. V. Skuratov, A. V. Krasheninnikov, P. B. Sorokin, and L. A. Chernozatonskii, Nanoscale **10**, 14499 (2018).
18. L. A. Chernozatonskii, L. Yu. Antipina, and D. G. Kvashnin, JETP Lett. **111**, 235 (2020).
19. B. Sahu, H. Min, A. H. MacDonald, and S. K. Banerjee, Phys. Rev. B **78**, 045404 (2008).
20. T.-T. Vu, T.-K.-Q. Nguyen, A.-H. Huynh, T.-K.-L. Phan, and V.-T. Tran, Superlatt. Microstruct. **102**, 451 (2017).
21. J. W. Gonzalez, H. Santos, E. Prada, L. Brey, and L. Chico, Phys. Rev. B **83**, 205402 (2011).
22. W. J. Yu and X. Duan, Sci. Rep. **3**, 1248 (2013).
23. G. I. Márk, arXiv:2004.10046 [physics:quant-ph] (2020).
24. A. Mayer, Carbon **42**, 2057 (2004).
25. G. I. Márk, P. Vancsó, L. P. Biró, D. G. Kvashnin, L. A. Chernozatonskii, A. Chaves, K. Yu. Rakhimov, and P. Lambin, in *Fundamental and Applied Nano-Electromagnetics,* Ed. by A. Maffucci and S. A. Maksimenko (Springer Netherlands, Dordrecht, 2016), p. 89.
26. G. I. Márk, P. Vancsó, P. Lambin, C. Hwang, and L. P. Biro, J. Nanophoton. **6**, 061718 (2012).
27. P. Vancsó, G. I. Márk, P. Lambin, A. Mayer, Y.-S. Kim, C. Hwang, and L. P. Biró, Carbon **64**, 101 (2013).
28. P. Vancsó, G. I. Márk, P. Lambin, A. Mayer, C. Hwang, and L. P. Biró, Appl. Surf. Sci. **291**, 58 (2014).
29. G. I. Márk, L. P. Biró, and J. Gyulai, Phys. Rev. B **58**, 12645 (1998).
30. G. I. Márk, P. Vancsó, C. Hwang, P. Lambin, and L. P. Biró, Phys. Rev. B **85**, 121402(R) (2012).
31. S. Plimpton, J. Comput. Phys. **117**, 1 (1995).
32. S. J. Stuart, A. B. Tutein, and J. A. Harrison, J. Chem. Phys. **112**, 6472 (2000).

Translated by K. Kugel